Journal of Sound and Vibration (1998) **216**(3), 435–459
Article No. sv981736

ON THE MODELLING OF FRICTION OSCILLATORS

N. Hinrichs, M. Oestreich and K. Popp

Institute of Mechanics, *University of Hannover*, *Appelstrasse* 11, 30167 *Hannover*, *Germany*

(*Received* 26 *January* 1998, *and in final form* 20 *April* 1998)

In the present paper the dynamics of a non-smooth friction oscillator under self- and external excitation are investigated. The rich bifurcational behaviour predicted by numerical simulations is compared to experimental results. In order to predict the period and amplitude of the friction induced vibrations, the friction force can be modelled by means of friction characteristics. A more detailed look at the non-smooth transition points of the trajectories shows that an extension of the friction model is necessary. For that purpose a bristle model, a friction contact with tangential stiffness and damping and a stochastic friction model are investigated.

1. INTRODUCTION

In everyday life one becomes aware of friction only at such times as when somebody slips on polished stairs or falls to the pavement having slipped on ice. A detailed analysis shows that friction results in a nonsmooth non-linearity which is abundant in nature, machines, structures, transportation systems and other processes. The economic losses due to friction and wear have been estimated at 5% of gross national product.

In driven systems friction often leads to stick–slip vibrations. This non-linear effect shows up in many kinds of engineering systems and also in everyday life. Examples are the stick–slip oscillations of the string of a violin, a singing wine glass, creaking doors or grating brakes (see Figure 1).

If somebody looses his footing on the ice, from one moment to the next his motion seems to obey different laws. Similar to this case also for friction induced self-sustained oscillations different equations are valid for the stick and the slip

Figure 1. Examples of stick–slip vibrations.

0022–460X/98/380435 + 25 $30.00/0

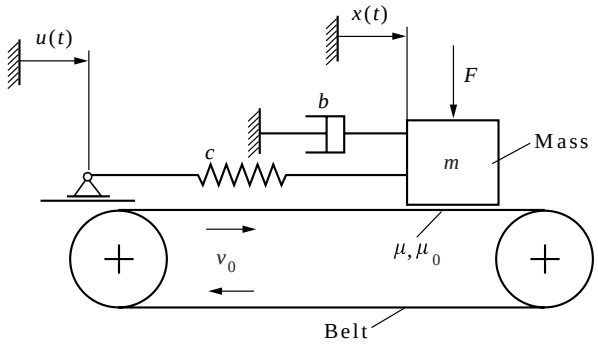

Figure 2. Model of a friction oscillator with self- and external excitation.

mode. Caused by the switch between these two equations, dynamical systems with friction are often called non-smooth systems where the friction characteristic is a set-valued mapping which yields discontinuities in the accelerations. So, usual dynamical systems theory for smooth systems is not applicable to a frictional system.

Already a one-degree-of-freedom self-excited friction oscillator shows a robust limit cycle, which yields noise and wear for the examples shown in Figure 1. The robust limit cycle of stick–slip vibrations can be broken up by an external harmonic excitation. The resulting system behaviour can exhibit rich bifurcational behaviour and also chaos. For chaotic trajectories of the stick–slip oscillations the energy shows a broad band spectrum. For the given examples this would lead to a reduced noise level and smaller amount of wear.

In the following the dynamical behaviour of a friction oscillator with simultaneous self- and external excitation will be analyzed by numerical simulations and experiments.

2. NUMERICAL INVESTIGATION OF A FRICTION OSCILLATOR

2.1. MECHANICAL MODEL OF A FRICTION OSCILLATOR

The mechanical model of a friction oscillator with simultaneous self- and external excitation is shown in Figure 2.

The following notation is used: mass m, spring constant c, displacement of mass $x(t)$, excitation $u(t) = u_0 \cos \Omega t$, damping constant b, normal force F_N, belt speed v_0. The friction force, in the following denoted by F_R, depends on the relative velocity $v_r = v_0\text{-}\dot{x}$ between the belt and the mass. For $u(t) = 0$ one has the case of pure self excitation. Then the oscillator can be used as a model for bowed instruments for example. The moving belt serves as an energy source and replaces the bow. The mass-spring-damper system models the vibrating string. The energy is transferred from the belt to the oscillator by means of friction with a decreasing characteristic (colophony), cp. [1]. For $u(t) \neq 0$ an additional external excitation is given.

The equation of motion reads

$$m\ddot{x}(t) + b\dot{x}(t) + cx(t) = F_R(v_r) + cu_0 \cos \Omega t. \tag{1}$$

Using the normalized time

$$\tau = \omega_0 t, \qquad \omega = \sqrt{\frac{c}{m}}, \qquad (*)' = \frac{\mathrm{d}(*)}{\mathrm{d}\tau} = \frac{(\dot{*})}{\omega_0}, \qquad v_r = v_0 - \omega_0 x', \tag{2}$$

and the damping ratio $D = b/(2\sqrt{\mathrm{cm}})$ as well as the frequency ratio $\eta = \Omega/\omega_0$ the system equation (1) can be transformed to

$$x''(\tau) + 2Dx'(\tau) + x(\tau) = \frac{F_R(v_r)}{c} + u_0 \cos \eta\tau. \tag{3}$$

For the following numerical investigations it is assumed that $D = 0$ and $\omega_0 = 1$ (rad/s). For the description of the friction force a suitable friction model has to be formulated.

2.2. FRICTION MODEL

Friction characteristics are a common way to describe the dependence of the friction force on the relative velocity. During the slip mode ($v_r \neq 0$) the friction force can be determined via the friction coefficient $\mu(v_r)$.

$$F_R(v_r) = \mu(v_r) F_N \operatorname{sgn}(v_r). \tag{4}$$

During the stick mode ($v_r = 0$) the friction force reads $F_F = c(x - u)$ and is bounded by

$$|F_R| = \mu(\omega_0 x' = v_0) F_N. \tag{5}$$

Figure 3 shows three different friction characteristics (in the following denoted by I, II and III). The friction coefficient $\mu(v_r) = |F_R(v_r)|/F_N$ is plotted as a function of the relative velocity.

For friction characteristic I the friction coefficient does not differ during the stick mode and the slip mode. Friction characteristic II is the well-known friction characteristic of Coulomb–Amontons and friction characteristic III is a spline

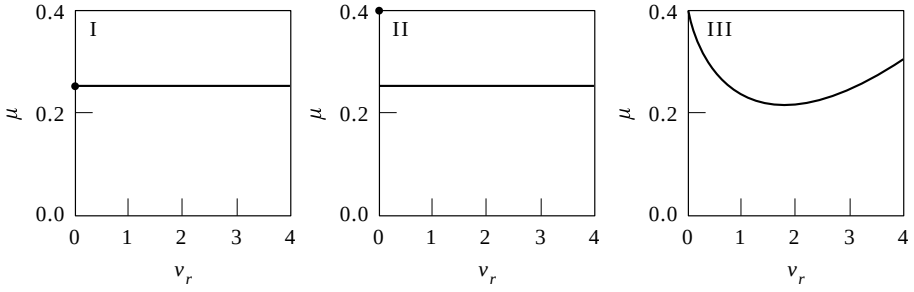

Figure 3. Used friction characteristics. I: $\mu_0 = \mu(v_r \neq 0) = 0{\cdot}25$; II: $\mu_0 = 0{\cdot}4$, $\mu(v_r \neq 0) = 0{\cdot}25$; III: $\mu_{\mathrm{III}}(v_r) = 0{\cdot}3/1 + 1{\cdot}42|v_r| + 0{\cdot}1 + 0{\cdot}01v_r^2$.

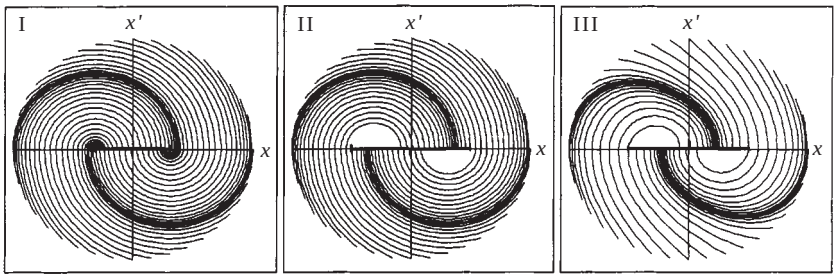

Figure 4. Phase portraits for free vibrations of the friction oscillator.

approximation of a measured friction characteristic, cf. [2]. In general the friction characteristic is not known in advance and changes with time. For that reason in the following the system behaviour is analyzed for the different friction characteristics.

2.3. SYSTEM BEHAVIOUR OF THE FRICTION OSCILLATOR FOR FREE VIBRATIONS

In Figure 4 the system behaviour of the friction oscillator without self- and external excitation ($u_0 = 0$, $v_0 = 0$) is shown for different initial conditions and for the friction characteristics, I–III. With increasing time a point on the trajectories in the phase plane travels to the right in the upper half plane ($x' > 0$) and to the left in the lower half plane ($x' < 0$). After a short time the mass sticks on the ground in the region of the thick line $[-\mu(v_r = 0)F_N/c \leqslant x \leqslant \mu(v_r = 0)F_N/c]$. For characteristics II and III there exists a dead zone, which is caused by the decrease of the friction characteristics.

2.4. SYSTEM BEHAVIOUR OF THE FRICTION OSCILLATOR WITH SELF EXCITATION

In the case of pure self excitation ($u_0 = 0$, $v_0 \neq 0$) one can observe stick–slip vibrations for the friction oscillator. Figure 5 shows the phase portraits for the friction characteristics I–III. For characteristics I and II during the slip mode the solution is represented by arcs of circles corresponding to the solution of the linear equation. Due to the decreasing characteristic for friction characteristic III self excitation occurs. As a typical feature of systems with friction the transients for the three characteristics decay very fast if the initial values lie outside the limit cycles, cf. Figure 5.

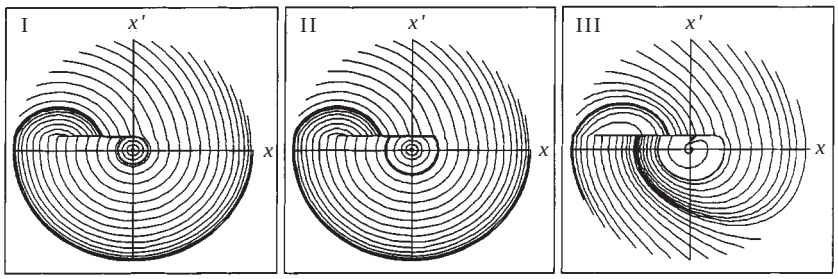

Figure 5. Phase portrait for self excited vibrations of the friction oscillator.

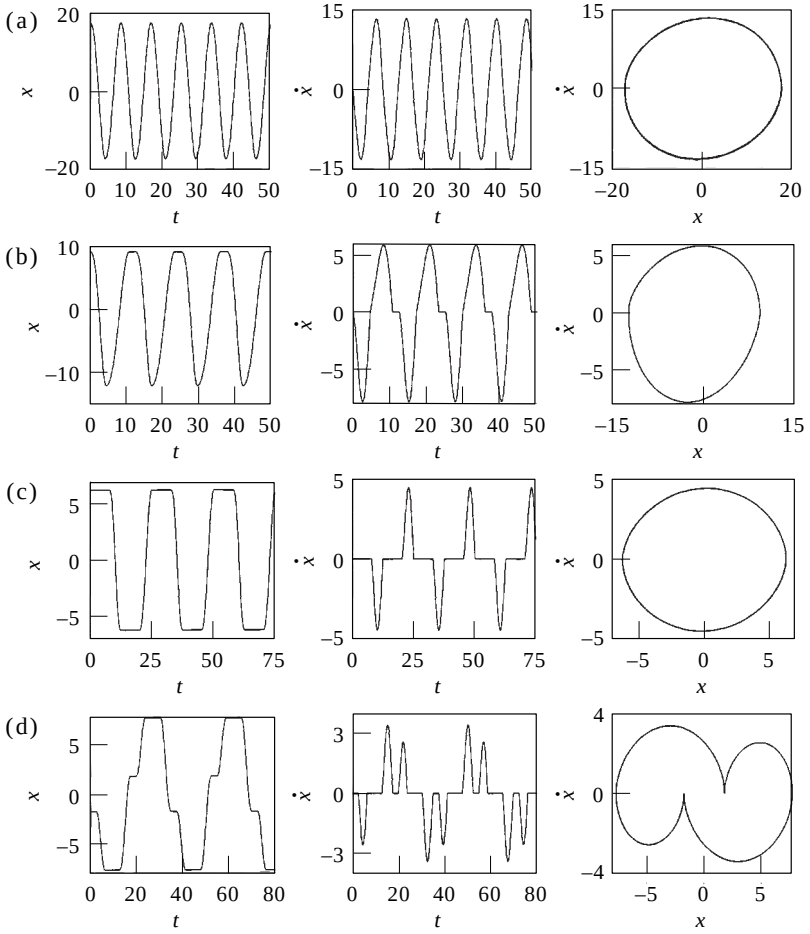

Figure 6. Friction oscillator with external excitation (friction characteristic II, $F_N/c = 10$ [m], $u_0 = 8$ [m]). (a) $\eta = 0{\cdot}75$, (b) $\eta = 0{\cdot}50$, (c) $\eta = 0{\cdot}25$, (d) $\eta = 0{\cdot}20$.

2.5. SYSTEM BEHAVIOUR OF THE FRICTION OSCILLATOR WITH EXTERNAL EXCITATION

The harmonically excited linear oscillator with a non-smooth friction characteristic ($u_0 \neq 0$, $v_0 = 0$) exhibits qualitatively different types of motions. For small amplitudes u_0 of the excitation,

$$u_0 \leqslant \mu(v_r = 0)F_N/c,$$

displacements in the range

$$-\mu(v_r = 0)F_N/c + u_0 < x < \mu(v_r = 0)F_N/c - u_0$$

are stable equilibrium positions. For larger values of the excitation amplitude depending on the bifurcation parameter η the friction oscillator shows motions without stop [Figure 6(a)], motions with one stop [Figure 6(b)], motions with two stops [Figure 6(c)] and motions with four stops [Figure 6(d)], where stop means $\dot{x}(t) = 0$ for a finite time. The qualitative change of the system behaviour for small

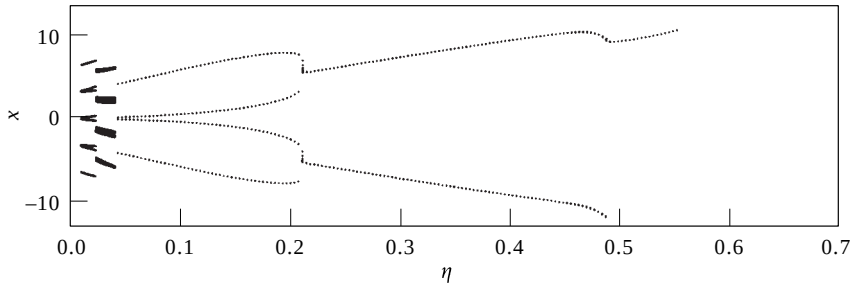

Figure 7. Bifurcation diagram showing the transition points from stick to slip for different excitation frequencies (friction characteristic II, $F_N/c = 10$ [m], $u_0 = 8$ [m]).

changes of one system parameter can be summarized by means of a bifurcation diagram (see Figure 7). This plot shows the displacement x of the mass at the stop as a function of the frequency ratio η. Obviously for $\eta > 0{\cdot}55$ no regions of sticking exist in the range investigated. The number of stops increase with decreasing η. Further numerical investigations can be found in references [3, 4]. The previous investigations show non-linear effects, so a robust limit cycle for self excitation and a sensitive parameter dependence for the external excitation occur. Because of the non-linearity of the system these two effects cannot be superposed. In the following the system behaviour for simultaneous self- and external excitation ($u_0 \neq 0$, $v_0 \neq 0$) is investigated.

2.6. SYSTEM BEHAVIOUR OF THE FRICTION OSCILLATOR WITH SELF- AND EXTERNAL EXCITATION

The system behaviour for a fixed set of bifurcation parameters u_0, F_N/c and η is represented by the phase trajectories. Figure 8 shows different types of phase plane plots. In contrast to the system with pure self excitation the system with additional external excitation exhibits one-periodic solutions [Figure 8(a)], two-periodic solution [Figure 8(b)], higher-periodic solutions and also chaotic system behaviour [Figure 8(c)]. For a more global examination of the bifurcational behaviour of the system, representative points of the trajectories for each set of bifurcation parameters have been extracted. In the bifurcation diagram the displacement x_A (transition point from stick to slip) is plotted as a function of the bifurcation parameter η. Figure 9(II) shows the results for friction characteristic

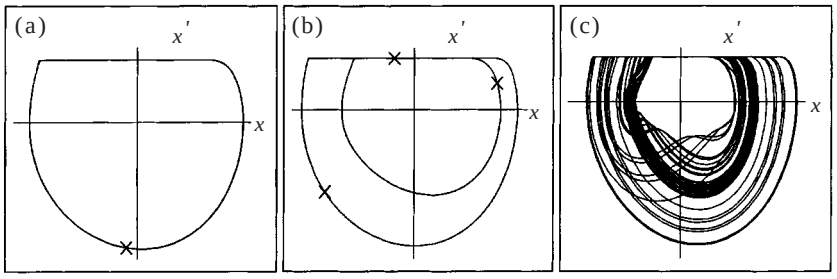

Figure 8. Phase portraits (friction characteristics III). (a) $\eta = 0{\cdot}9$, $F_N/c = 10$ [m], $u_0 = 0{\cdot}5$ [m]; (b) $\eta = 1{\cdot}15$, $F_N/c = 10$ [m], $u_0 = 0{\cdot}5$ [m]; (c) $\eta = 1{\cdot}915$, $F_N/c = 10$ [m], $u_0 = 1{\cdot}0$ [m].

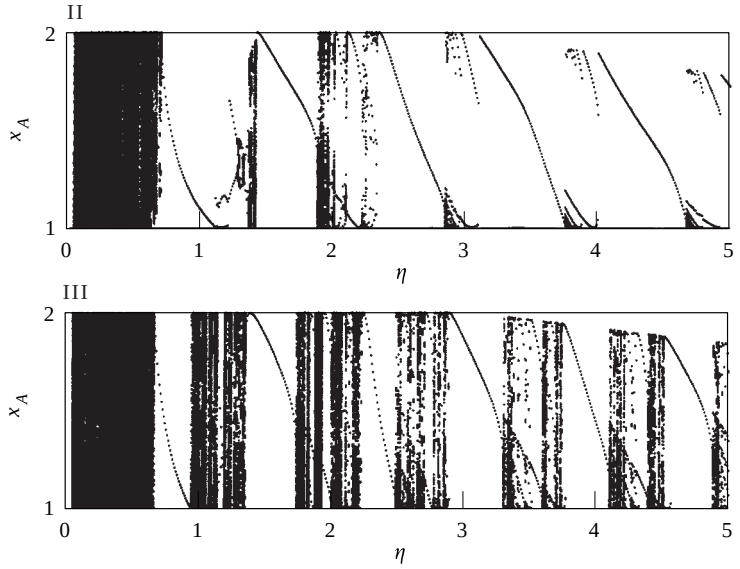

Figure 9. Bifurcation diagrams (friction characteristic II, III) $F_N/c = 10$ [m], $u_0 = 0{\cdot}5$ [m].

II and Figure 9(III) for friction characteristic III. In the bifurcation diagrams one can distinguish one-periodic and higher-periodic solutions. For large excitation amplitudes u_0 also period doubling cascades have been found, e.g., [5, 6].

In order to give an overview of the system behaviour depending on two bifurcation parameters, parameter maps have been calculated, cf. Figure 10. The periodicity of the solutions is visualized by a colour code. In the parameter map regions of one-periodic orbits are marked in light grey, regions of five- or higher-periodic orbits including chaos are represented in black. So, for each set of bifurcation parameters F_N/c and η for fixed $u_0 = 0{\cdot}5$, the corresponding system behaviour can be determined. Parameter maps for fixed F_N/c and variation of η and u_0, showing the well-known Arnold tongues can be found for example in reference [6].

Comparing the results gained for the different friction characteristics shows that the global bifurcational behaviour is similar. For small values of η the limit curves of the lowest two light grey regions are nearly identical. However, for high values of η and F_N/c the tongues of high-periodic motions disappear for friction characteristic II. The number of tongues characterizing orbits of constant periodicity is smaller for characteristic II than for characteristic III.

3. FURTHER INVESTIGATIONS

In general bifurcation and stability analysis for smooth non-linear systems is done by means of numerical tools such as BIFPACK or PATH. In order to apply those tools for the non-smooth friction oscillator the friction characteristics have to be smoothed [1, 7]. A verification of this smoothing procedure for stiff smoothing functions has been done comparing the bifurcation behaviour of the original non-smooth and the smoothed system. It turns out that both results agree

very well if the smoothed friction characteristic has a steep slope in the origin. Furthermore, it is possible to reduce the dynamics of the friction oscillator to a one-dimensional map. This mapping approach is based on a Poincaré map that determines the points in which the trajectories leave the stick plane in the three-dimensional state space. The reason for the reduction of the dynamics is an additional equation for the end of the stick phase. This equation gives a relation between the three state variables.

In reference [5] it has been shown that the mapping approach is very helpful to gain insight into the different routes to chaos like period doubling and intermittency. Additionally, bifurcation analysis and the determination of Lyapunov exponents has been done for the non-smooth system.

In addition, the cell mapping approach has been applied [8]. Results are the domains of attraction for co-existing solutions and the transient times for different initial conditions.

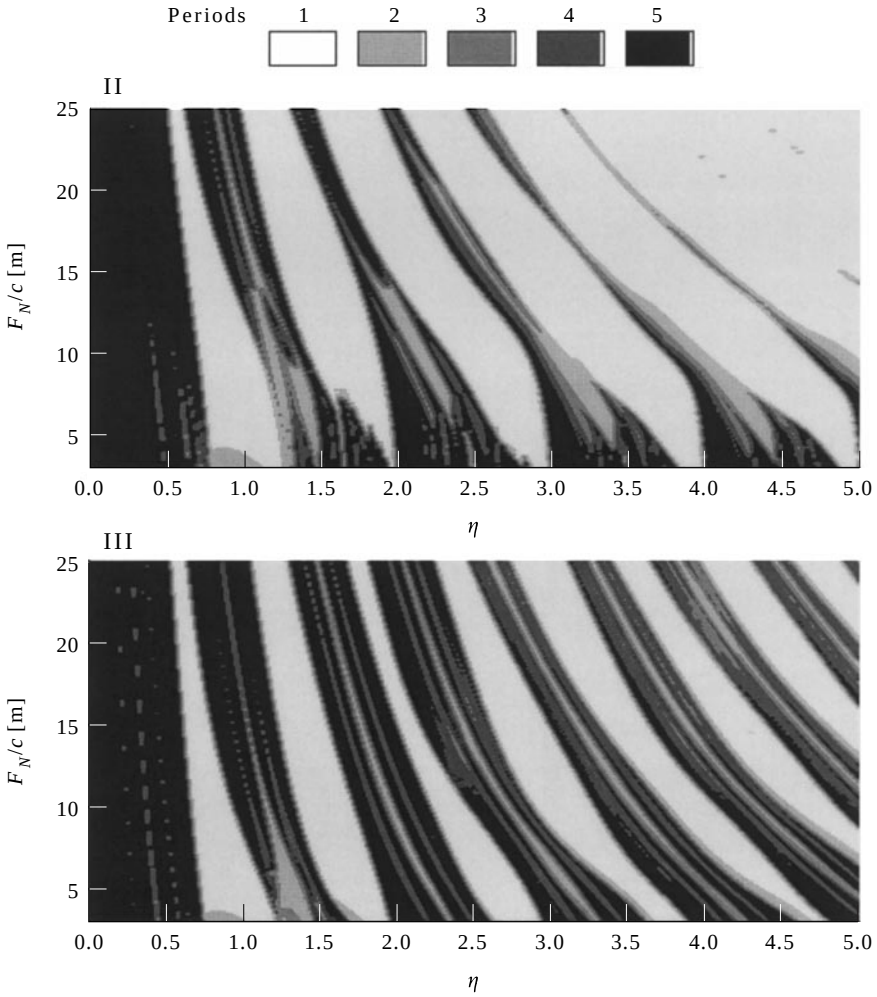

Figure 10. Parameter maps (friction characteristic II, III): $u_0 = 0{\cdot}5$ [m].

Different techniques for the analysis of time series [9] of non-smooth mechanical systems have been tested in references [10] and [6]. Also, signal and model-based algorithms have been applied for the determination of the embedding dimension using the method of False Nearest Neighbours, the Lyapunov exponents and for the reconstruction of the attractor.

In the following the chosen models for the system and the friction force will be verified by means of experiments.

4. EXPERIMENTAL SETUP

For the experimental investigation of the friction oscillator a one-degree-of-freedom oscillator has been chosen consisting of the pendulum, 1, which is supported by two air-pressurized bearings, 2 and 3 [see Figure 11(a)]. Additionally to the rotational degree of freedom (axis ξ) the pendulum can be moved horizontally in the direction of ξ. The pendulum is equipped with two springs, 4, [Figure 11(b)]. In the case of the experimental investigations, the self excitation is done by means of a rotating shaft, 5, with disk, 6, instead of the belt. The shaft is supported by two bearings, 7. (So, in order to investigate metal as contact material the model Figure 2 with a translational degree of freedom has been transformed to a rotational oscillator). In the setup Figure 11(b) the shaft does not have any contact with the pendulum and the air bearings. The pendulum is connected to the cylindrical friction body, 9, by means of the support unit, 8, [Figure 11(c)]. The whole pendulum with the friction body is pulled by additional ropes and dead masses fixed at the traverse, 10, in direction of ξ and pressed against the rotating disk. Changing the friction body, 9, and the disk connected with the shaft different friction materials can be investigated. All contact forces, i.e., the friction and the normal forces, are measured directly by means of a three component force transducer.

The external excitation of the base of the spring (Figure 2) is transformed to a force excitation which can be done without rigid body contact by means of a magnetic excitation, cf. reference [11]. Measurements during the free oscillations of the pendulum without friction contact lead to a damping coefficient $D < 0.005$ including the material damping of the springs and the damping of the air bearings. During the measurements the displacement and the velocity of the end point of one arm of the pendulum are sensed by a laservibrometer. Incorporating the geometric properties and the identified system parameters the system equation can be transformed to equation (1). For the following results the transformed parameters are given in the legend of the figures. If not specified elsewhere the axes are scaled in the following way: time t in [s], forces in [N], displacement in [mm] and velocity in [mm/s].

5. DETERMINATION OF THE FRICTION MODEL

In order to determine an appropriate friction model in the first step the rotational degree of freedom is fixed by means of an additional pair of air bearings. The disk is driven with constant velocity. For a set of measurements with different

velocities the friction coefficient is calculated by the ratio of the measured time dependent friction force and the normal force. This time dependent friction force exhibits a random feature which—in a first approximation—can be supposed to be Gaussian (see also references [7, 12]). The mean value (solid line) and the standard deviation (dashed line) are plotted for different relative velocities [see Figure 12(a)].

The friction characteristic decreases for increasing relative velocity. In order to avoid a change of the contact conditions the contact has been cleaned during the time consuming tests which results in small jumps of the mean values. In order to compare the friction characteristics with those given in the literature and to insert them into the simulation software a curve fit has also been done. Here a fit with an exponential function of the form

$$\tilde{\mu}(v_r) = b_0 + b_1 \, \mathrm{e}^{b_2 v_r} \tag{6}$$

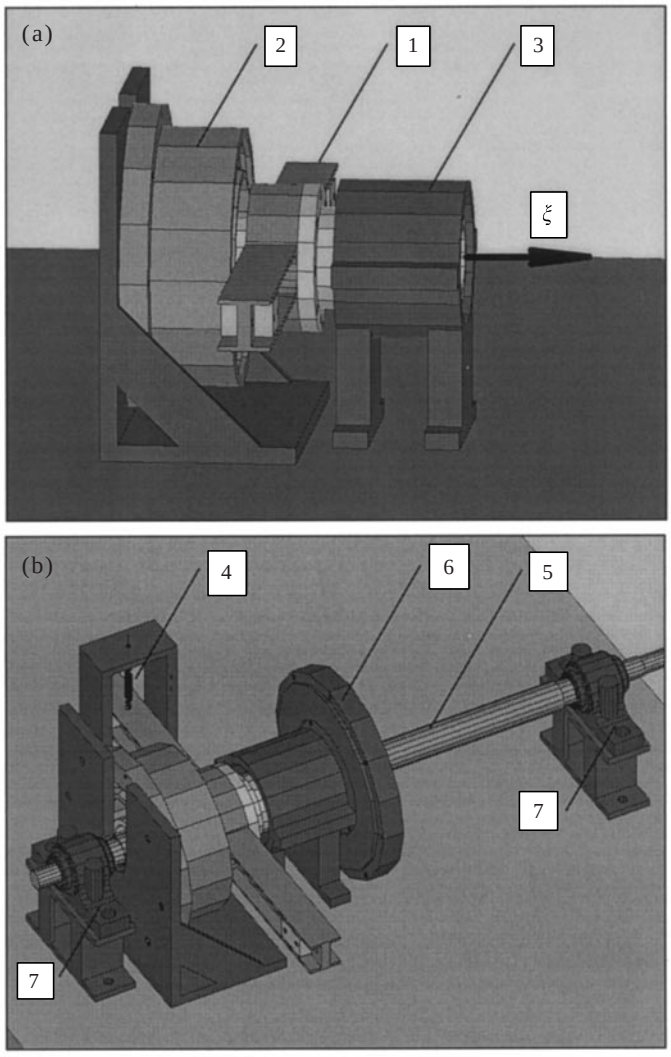

Fig. 11(a), (b).

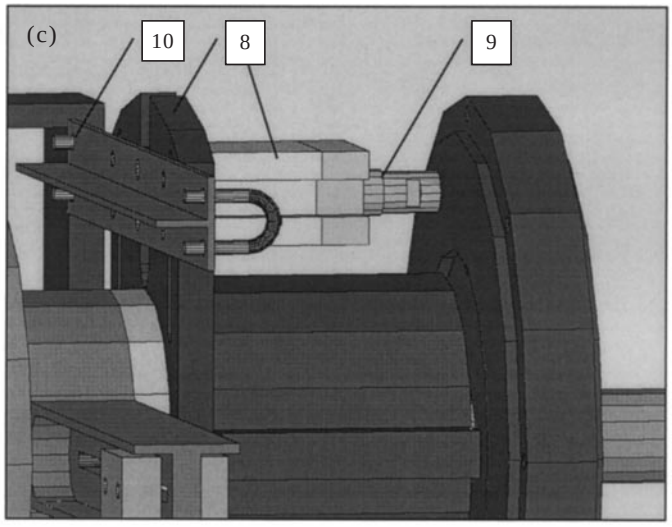

Fig. 11(c).

Figure 11. Experimental setup.

seems to be most accurate. A comparison of the friction characteristics for different contact materials and normal forces can be found in reference [7].

6. EXPERIMENTAL RESULTS

6.1. FREE VIBRATIONS

The results of the measurements for the friction oscillator performing free oscillations are plotted in Figure 13. In the friction characteristic for the friction materials steel–steel there is no jump at the transition point from stick to slip. Corresponding to the results from the simulation Figure 4(I) this means that there is no dead zone in the phase curves (see Figure 13). Due to the non-smooth model for the friction force all the displacements in the range of the thick line are stable equilibrium positions. In the measured force signal [Figure 13(c)], the sign of the friction force jumps for a change of the relative velocity ($t = 0{\cdot}23$ [s], $t = 0{\cdot}35$ [s]).

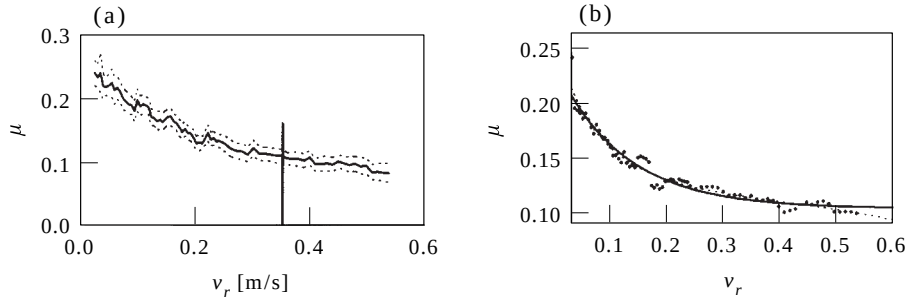

Figure 12. Measurements (materials: steel-brass): (a) friction characteristic, (b) spline-approximation. Key: ...., mean value; ——, exponential function; ----, polynomial function.

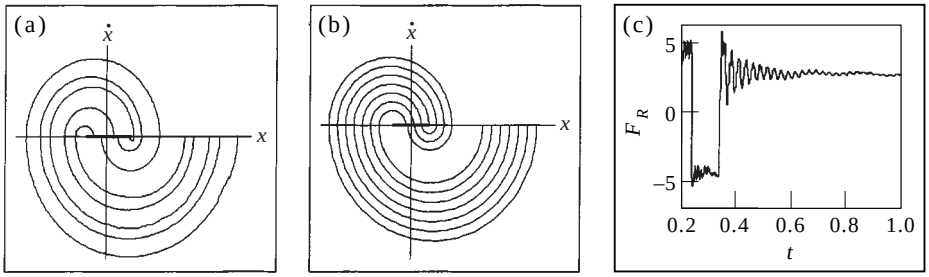

Figure 13. System behaviour: Free oscillations (materials: steel–steel): (a) measurement, (b) simulation, (c) friction force ($F_N = 18$ [N], $c = 3956$ [N/m], $b = 0{\cdot}768$ [Ns/m], $m = 6{\cdot}08$ [kg]).

After a short slip phase, for $t > 0{\cdot}35$ [s] the friction body sticks to the disk. The friction force oscillates around a mean value of 3[N] which is equal to the spring force in the equilibrium position, see section 7.

In the following the disk is driven with constant angular velocity.

6.2. SYSTEM BEHAVIOUR FOR PURE SELF EXCITATION

The amount of energy transferred by self excitation from the driven disk to the oscillator depends on the magnitude of the decrease of the friction characteristics between sticking and slipping. Like the model shown in Figure 2 the experiments are damped, so in order to get self excitation the energy transferred from the disk to the oscillator must be larger than the energy dissipated during one period of the oscillations. Measurements have shown, that the decrease of the friction characteristics for the friction materials steel–polyurethane is larger than that for the materials steel–aluminum, steel–brass and steel–bronze, So, this pair of materials leads to the largest limit cycle amplitude. Additionally, the contact area is treated with colophony.

The measured phase curve, Figure 14(a), for pure self excitation consists of a stick line representing constant velocity and the part of an ellipse during the slip mode. In contrast to the simulations, see section 2, the velocity during the stick mode oscillates slightly due to asynchronisms of the angular velocity of the driving shaft and small play in the gear box. For the transition from slip to stick there are small overshoots of the velocity signal.

Due to the stochastic component of the friction coefficient the transition point from the stick to slip differs slightly. So, in contrast to the simulations the system behaviour for the measurements is not periodic. In Figure 14(b) the time dependent friction force is plotted. For the transition from stick to slip ($t = 0{\cdot}9$ [s]) the friction force jumps. The next jump occurs for the transition from slip to stick ($t = 1{\cdot}0$ [s]). This jump in the contact force results in decaying oscillations of the friction force. The period of those oscillations equals the period of the transients in the velocity signal. Figure 14(c) shows the identified friction characteristic that exhibits a decrease for the transition from stick to slip.

For pure self excitation there is no bifurcational behaviour. In order to carry out experiments for the bifurcational behaviour of the friction oscillator external excitation is done by means of the magnetic excitation.

6.3. SYSTEM BEHAVIOUR OF THE FRICTION OSCILLATOR FOR PURE EXTERNAL EXCITATION

The numerical simulations of the system behaviour in Figure 6 have revealed the bifurcational behaviour of the friction oscillator with pure external excitation. The results from the experiments are shown in Figure 15. The bifurcational parameter is the excitation frequency. One can observe motions without stop [Figure 15(a)], motions with one stop [Figure 15(b)], motions with two stops [Figure 6(c)] and motions with four stops [Figure 6(d)]. The results are qualitatively similar to the results gained from the simulations, cf. Figure 6. For the sticking mass a high frequency oscillation can be observed in the velocity signal.

The corresponding bifurcation diagram under variation of the frequency ratio η is presented in Figure 16. One can observe the bifurcation structure from solutions with one stop to solutions with multiple stops. A comparison with the bifurcation diagram from simulations (Figure 7) shows again a good agreement. The only difference is, that in the experiment the stochasticity of the friction force results in a cloud of points instead of a single point as in the simulations.

6.4. DISCUSSION OF THE RESULTS

A comparison of the results from measurements and simulations shows that the global system behaviour of the friction oscillator, i.e., the amplitude and the period of the oscillators, can be predicted by the simulations. The stochastic component of the friction coefficient, however, has not been included in the simulations yet. Moreover, the transients in the transition regimes from slip to stick do not occur in the simulations. A more detailed insight in the dynamics in this regime is given in the following. (System parameters Figures 17–19: $m = 6{\cdot}08$ [kg], $b = 0{\cdot}786$ [Ns/m], $c = 3956$ [N/m], $F_N = 5$ [N], $u_0 = 0{\cdot}65$ [mm]).

Figure 17 shows the experimental results for the system with pure external excitation and two stops during one period of the excitation. Due to the oscillations at the beginning of the stick phase, cp. the small twiggles in the phase curves Figure 17(a) for $\dot{x} = 0$ and the oscillations of the friction force [Figure 17(b)], the transition of the friction coefficient takes place in the range of $-v_H < \dot{x} < v_H$ (here $v_H \approx 1{\cdot}5$ [mm/s]) instead to $\dot{x} = 0$. The transition shows a

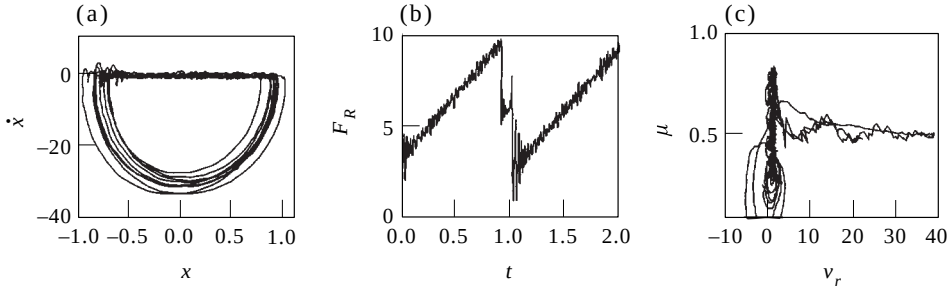

Figure 14. System behaviour for pure self excitation (materials: steel–polyurethane): (a) phase plane plot, (b) friction force, (c) friction characteristic.

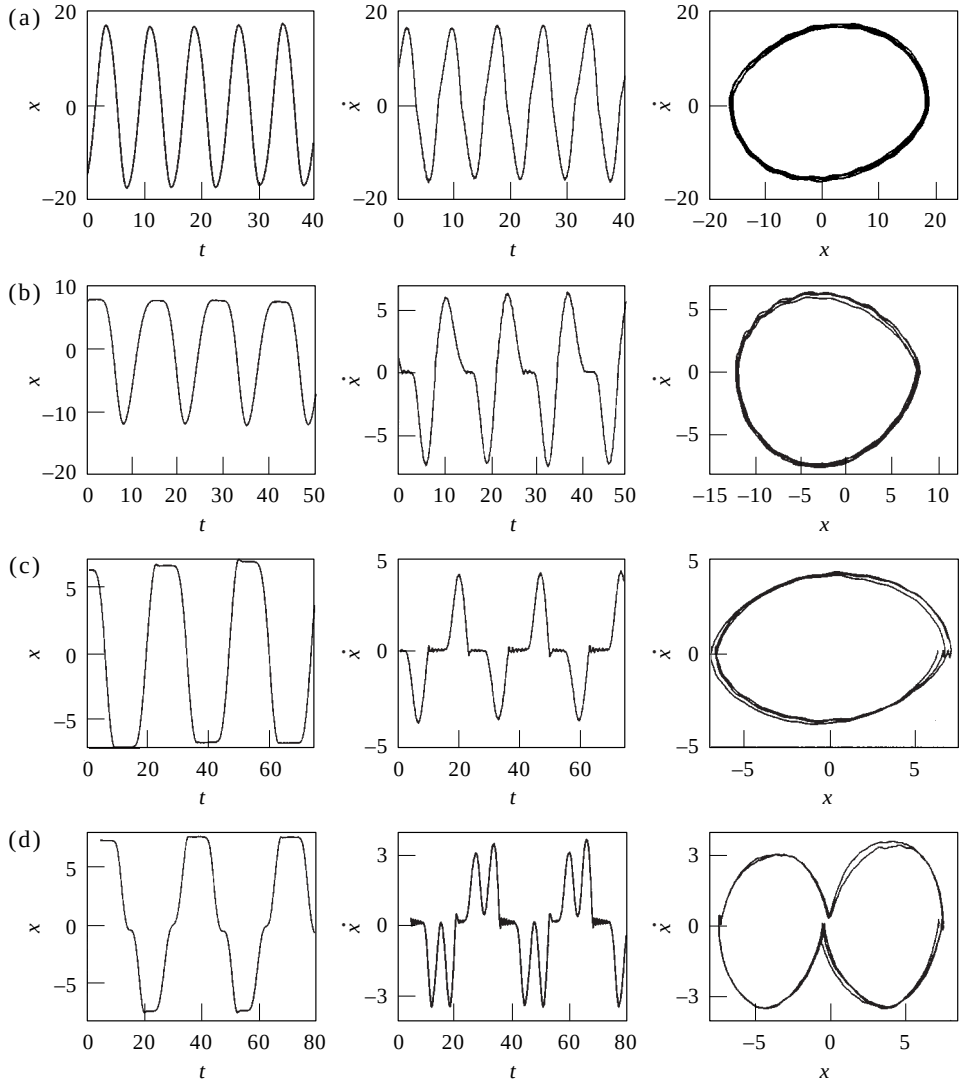

Figure 15. Friction oscillator with external excitation (experiments). (a) $\eta = 0{\cdot}5$, (b) $\eta = 0{\cdot}44$, (c) $\eta = 0{\cdot}28$, (d) $\eta = 0{\cdot}18$.

dynamic with limited stiffness. With an increase of the excitation frequency, cf. Figures 18(a) and (b), v_H and the hysteresis increase.

Due to the fact that the relative displacement and the relative velocity are sensed directly at the friction contact the dynamics of the pendulum cannot be responsible for the dynamics of the friction characteristic. A comparison of these results for the materials steel–polyurethane with the experimental results for stiffer contact materials (steel–aluminum) shows that the frequency of the transients is larger for the stiffer contact material [Figure 19(b)]. As a consequence the hysteresis is much smaller for the stiffer material. Results similar to those in Figure 19(b) can also be found in references [13] and [2].

These phenomena cannot be predicted by the model Figure 2. The following investigations have been initiated by the work in reference [13]. Thus, in the following the mechanical model will be extended so that both phenomena, the stochastic component of the friction coefficient and the dynamics of the friction characteristics, can be predicted.

7. EXTENDED MODELS

7.1. BRISTLE MODEL

For the contact of two rough technical surfaces the external forces lead to elastic and plastic deformations of the contacting asperities. The results presented in section 6.4 suggest that stiffness and damping for the deformations tangential to the slip plane have to be taken into account. Simplified models of single asperity contacts can be found in references [14] and [15]. Here the bristle model is used, cf. reference [16]. Instead of two elastic bunches of asperities this model supposes one bunch of rigid bristles and one bunch of elastic bristles with stiffness k_B, (Figure 20). The dependence of the friction coefficient on the relative velocity is modelled by means of the number of active bristles during the stick mode (M_H) and the slip mode (M_G). (A more detailed description of this model and the parameters is given in reference [7]).

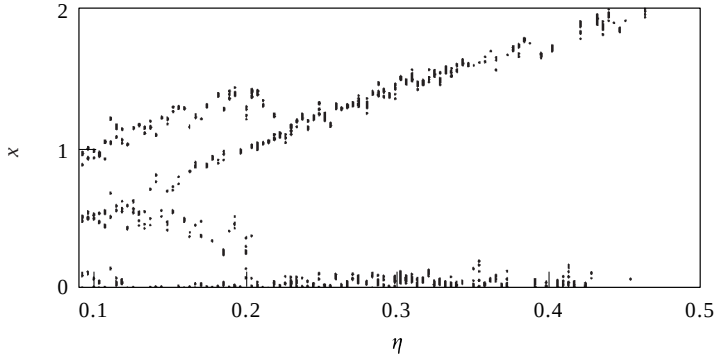

Figure 16. Bifurcation diagram showing measured transition points from stick to slip for different excitation frequencies (experiments, cf. simulations Figure 7).

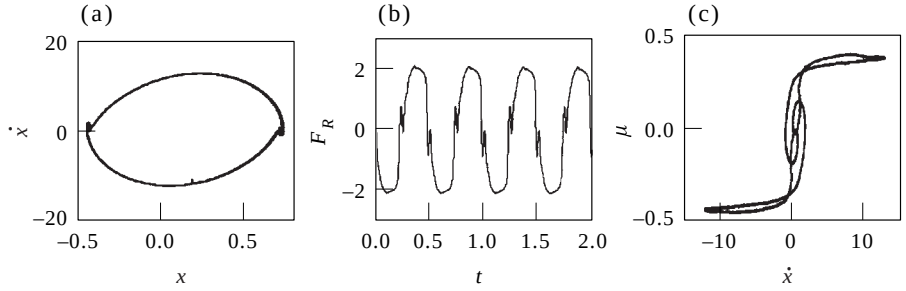

Figure 17. Dynamics at the transition from stick to slip (materials: steel–polyurethane), excitation frequency: $\Omega = 11{\cdot}5$ [1/s], (a) phase plane plot, (b) friction force and (c) friction characteristic.

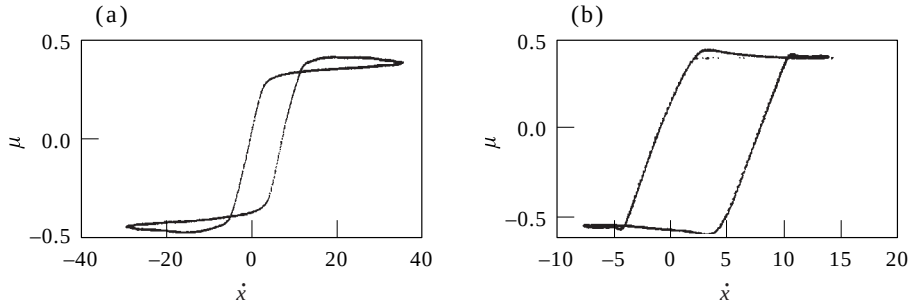

Figure 18. Change of the friction characteristic with a variation of the excitation frequency (materials: steel–polyurethane): (a) $\Omega = 37{\cdot}7$ [1/s], (b) $\Omega = 62{\cdot}8$ [1/s].

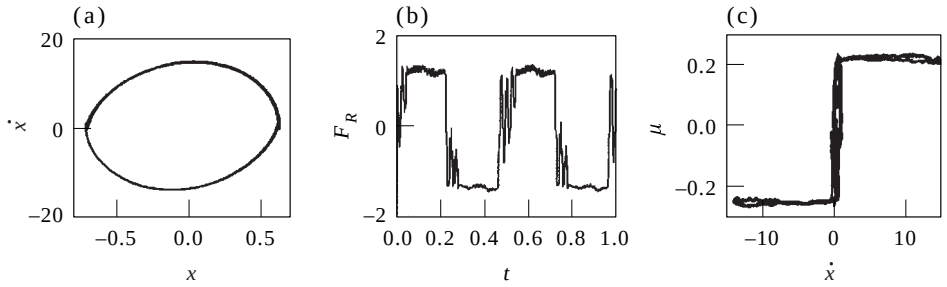

Figure 19. Dynamics of the friction contact during the stick–slip motion (materials: steel–aluminum; excitation frequency: $\Omega = 10{\cdot}5$ [1/s]): (a) phase plane plot, (b) friction force and (c) friction characteristic.

Figure 21(a) shows the system behaviour resulting from the simulations on the basis of the bristle model. Comparable to the measurements presented in reference [11] the maxima of the friction force vary from one transition point to another. The maximum of the friction force which equals the spring force depends on the position of the bristles at the start of the stick phase and varies from one transition point to the next [Figure 21(b)]. During the slip mode the friction force exhibits a stochastic component since due to the large displacements the contact for single

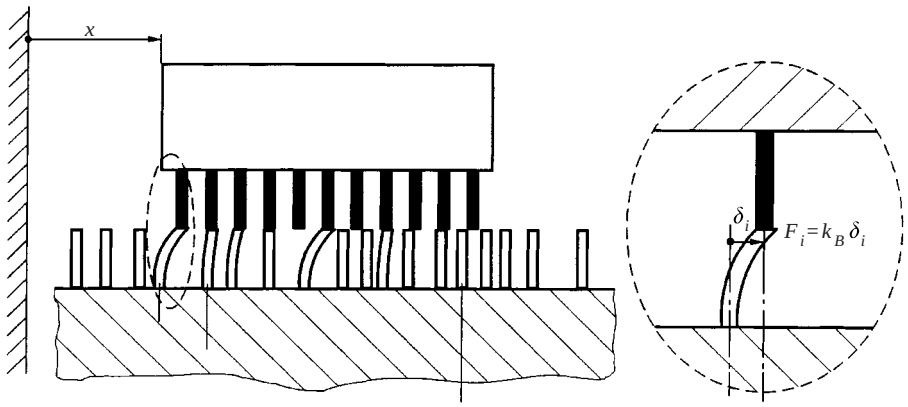

Figure 20. Bristle model.

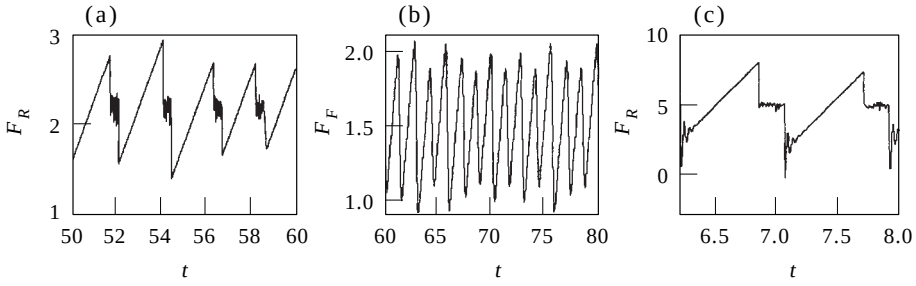

Figure 21. System behaviour of the friction oscillator with the bristle model: (a) friction force, (b) spring force and (c) friction force.

bristles are broken again and again and new contacts for statistically placed bristles have to be calculated. The stiffness (and the introduced damping) of the bristles leads to the transients at the transition from slip to stick, see Figure 21(c) and compare the experimental results, [7].

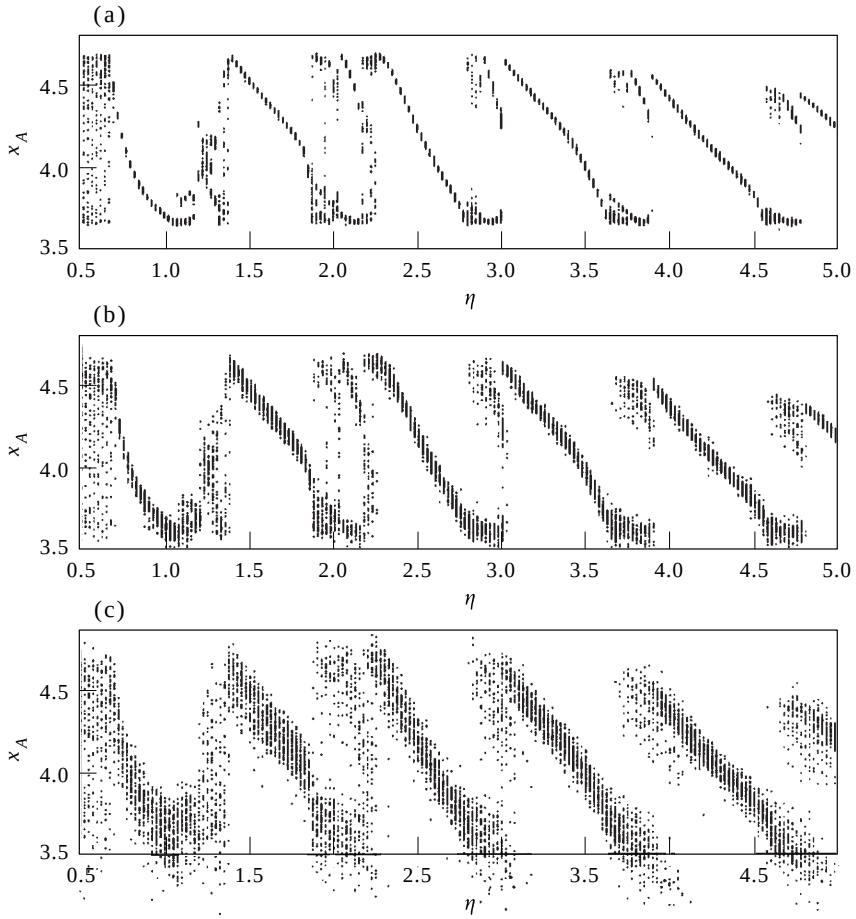

Figure 22. Bifurcational behaviour of the friction oscillator with the bristle model, cf. Figure 9 (II): $M_H = 24$, $M_G = 15$, (a) $m_B = 0{\cdot}0005$, (b) $m_B = 0{\cdot}001$, (c) $m_B = 0{\cdot}002$.

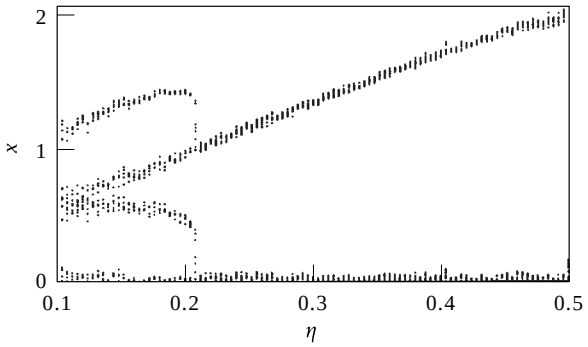

Figure 23. Bifurcation diagram of the friction oscillator with external excitation and simplified stochastic friction model, cf. Figure 16.

In the following the influence of the mean value for the stochastic bristle location m_B for each new bristle contact is studied. As expected for a small value of the mean value m_B the bifurcational behaviour approximates the results for the deterministic model Figure 9(II), see Figure 22(a). With an increase of the parameter m_B the points of the periodic solutions in Figure 9(II) are spread to a cloud of point, see Figures 22(b) and (c).

So, by means of the bristle model the phenomena discussed in section 6.4 can be predicted. However, the determination of a large number of transition points for each bristle leads to large computation times during integration. In the following the effect of the stochastic component and the dynamics of the friction characteristic will be separated and two simple models will be presented leading to smaller CPU-times than those required for the bristle model.

7.2. SIMPLIFIED STOCHASTIC FRICTION MODEL

The friction coefficient can be divided into a deterministic and a stochastic component:

$$\mu(v_r) = \mu_D(v_r) + \tilde{\mu}(v_r). \tag{7}$$

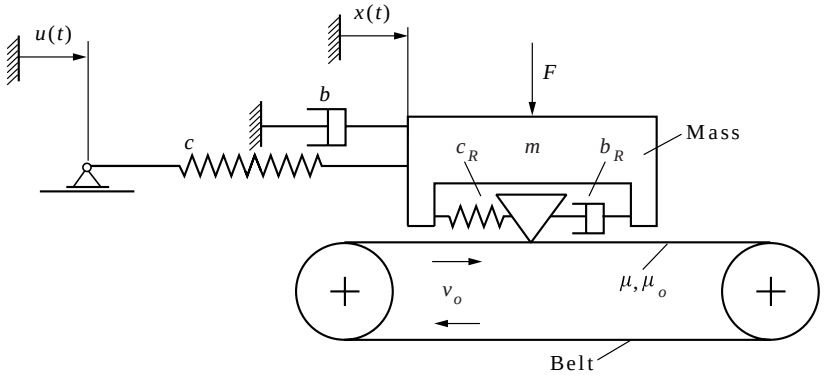

Figure 24. Model of the friction oscillator with contact damping b_R and contact stiffness c_R.

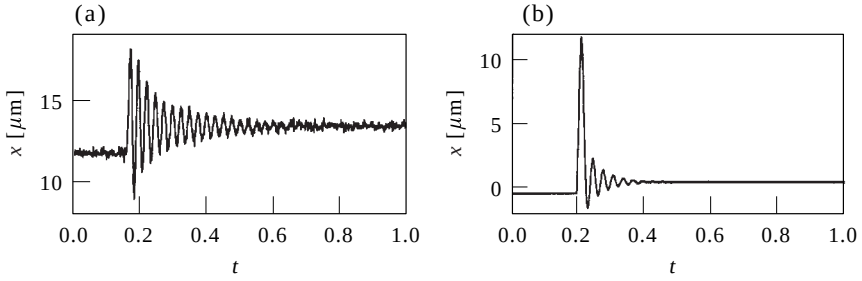

Figure 25. Free oscillations for impulse excitation of the sticking contact (materials: (a) steel–aluminium, (b) steel–polyurethane).

With the system parameter from sections 2 and 6 and a Gaussian distribution of the stochastic component $\tilde{\mu}(v_r)$ (zero mean value and standard deviation $\sigma = 0{\cdot}02$) the system behaviour for pure self excitation equals the results from the measurement (see Figures 16 and 23).

7.3. SIMPLIFIED MODEL FOR THE CONTACT STIFFNESS AND CONTACT DAMPING

A simple approach can be gained gathering all the bristles to one single spring (stiffness c_R) and a damper (damping coefficient b_R), cf. Figure 24 and reference [13]. The same model has been investigated in reference [17]. However the contact stiffness and damping has been introduced for reasons of the regularization of the non-smooth problem.

If the absolute displacement of the single asperity in Figure 24 is denoted by y, the system equation for the sliding block reads

$$m\ddot{x} + b\dot{x} + b_R(\dot{x} - \dot{y}) + cx + c_R(x - y) = cu. \tag{8}$$

The equation of motion for the asperity is given by

$$b_R(\dot{y} - \dot{x}) + c_R(y - x) = F_R. \tag{9}$$

The friction force during the slip mode ($\dot{y} \neq 0$) reads

$$F_R = \mu(v_r)F_N \operatorname{sign}(v_0 - \dot{y}) \tag{10}$$

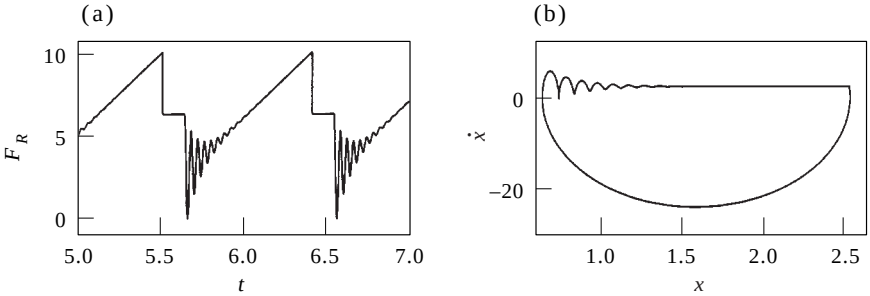

Figure 26. System response of the model with contact stiffness and damping for pure self excitation (materials: steel–polyurethane): $m = 6{\cdot}08$ [kg], $c = 3956$ [N/m], $b = 0{\cdot}768$ [Ns/m], $c_R = 150\,000$ [N/m], $b_R = 150$ [Ns/m], $\mu_0 = 0{\cdot}4$, $\mu = 0{\cdot}25$, $F_N = 25{\cdot}0$ [N], $v_0 = 0{\cdot}0025$ [m/s].

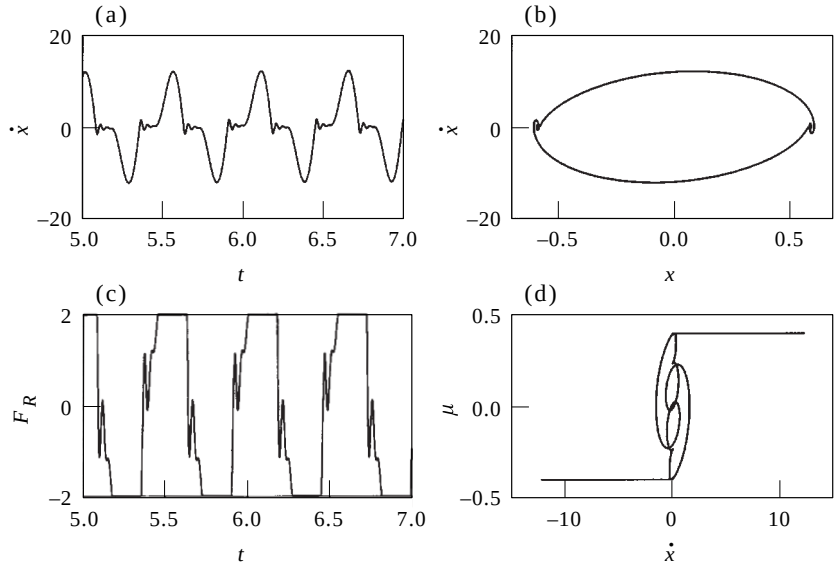

Figure 27. System response from simulations for pure external excitation (materials: steel–polyurethane): $m = 6{\cdot}08$ [kg], $c = 3956$ [N/m], $b = 0{\cdot}768$ [Ns/m], $c_R = 150\,000$ [N/m], $b_R = 400$ [Ns/m], $\mu_0 = 0{\cdot}4$, $\mu = 0{\cdot}4$, $F_N = 5{\cdot}0$ [N], $\Omega = 10{\cdot}50$ [1/s], $u_0 = 0{\cdot}00065$ [m], cf. Figures 15(c) and 17.

during the stick mode ($\dot{y} = 0$) the friction force equals

$$F_R = b_R(\dot{y} - \dot{x}) + c_R(y - x). \tag{11}$$

The transition point from stick to slip is reached for $F_R = \mu_0 F_N$, the slip mode finishes for $\dot{y} = v_0$. The still unknown stiffness c_R and the damping b_R can be measured applying a small impulse to the block, i.e., the pendulum in our experiments. (For the model in Figure 2 during the stick mode the displacement should equal zero!). Figure 25 shows the transient response of the systems for two different contact materials. From the frequency of the resulting oscillations the contact stiffness can be evaluated, while the decay of the oscillations determines

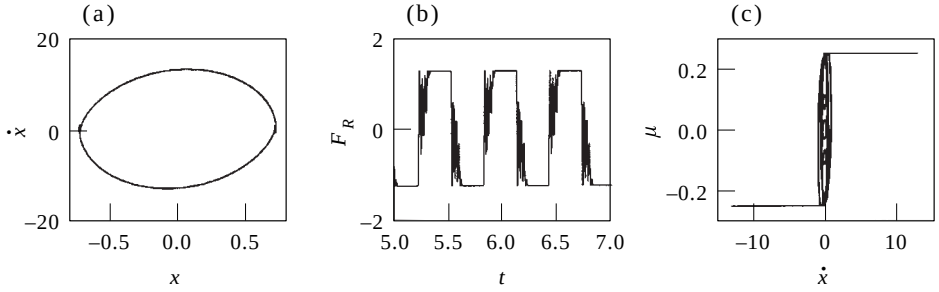

Figure 28. System response from simulations for pure external excitation (materials: steel–aluminum): $m = 6{\cdot}08$ [kg], $c = 3956$ [N/m], $b = 0{\cdot}768$ [Ns/m], $c_R = 400\,000$ [N/m], $b_R = 150$ [Ns/m], $\mu_0 = 0{\cdot}25$, $\mu = 0{\cdot}25$, $F_N = 5{\cdot}0$ [N], $\Omega = 10{\cdot}50$ [1/s], $u_0 = 0{\cdot}00065$ [m], cf. Figure 19.

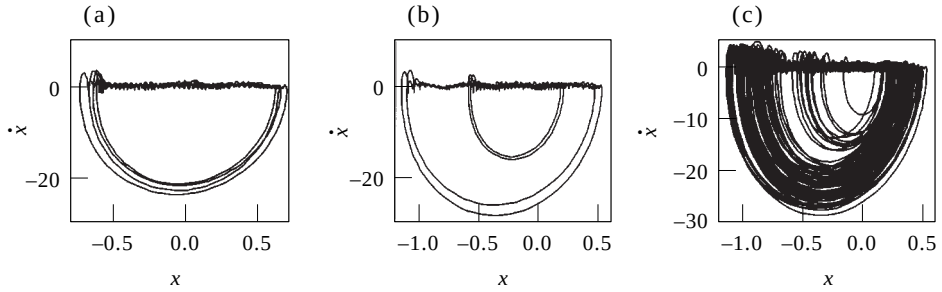

Figure 29. Phase plane plots of the friction oscillator for simultaneous self- and external excitation, (measurement): (a) $\Omega = 13{\cdot}8$ [1/s], (b) $\Omega = 15{\cdot}3$ [1/s], (c) $\Omega = 18{\cdot}7$ [1/s].

the damping. Figure 26 shows the results from the simulations on the basis of the identified contact parameters for pure self excitation.

One can see the overshoots of the friction force and the velocity known from the measurements, (Figure 14). The dynamics of the friction characteristic in the region of the transition from slip to stick can be predicted by means of the extension of the model. In Figure 27 (Figure 28) the results from the simulation for pure external excitation and the materials steel–polyurethane (steel–aluminum) are plotted, cf. also Figures 15(c) and 17 (Figure 19).

By means of the introduced extensions of the model Figure 2 the observed phenomena can be predicted. In the following the chosen model will be verified for the simultaneous self- and external excitation. Due to the sensitivity of the system responses to small changes to the parameters or changes to the initial

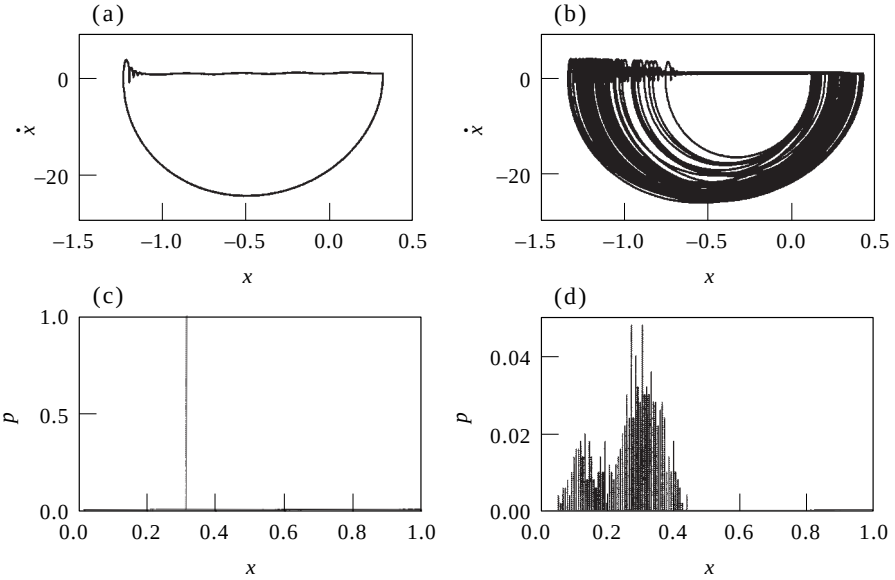

Figure 30. Probability p of a transition point from stick to slip for: (a), (c) deterministic friction model (section 7.3) and (b), (d) stochastic friction coefficient ($\sigma = 0{\cdot}015$).

conditions the comparison of the bifurcation diagrams from measurements and simulations is a very sensible tool for the verification of the chosen model.

8. COMPARISON OF THE SIMULATIONS BASED ON THE EXTENDED MODEL WITH THE EXPERIMENTS FOR SIMULTANEOUS SELF- AND EXTERNAL EXCITATION

The simultaneous self- and external excitation is done by means of driving the disk with constant velocity and exciting the pendulum by magnetic forces. Depending on the bifurcation parameters, here the excitation frequency and the disk speed, different types of motions can be observed. In the following we want to compare the bifurcational behaviour observed in the experiment with the results of our simulations based on the model Figure 24. The identified system parameters are: $m = 5{\cdot}632$ [kg], $b = 0{\cdot}768$ [Ns/m], $c = 5610$ [N/m], $v_0 = 0{\cdot}001$ [m/s], $u_0 = 0{\cdot}0005$ [m], $F_N = 14$ [N]; materials: steel–polyurethane. The "one-periodic" solution Figure 29(a) shows oscillations in the transition regime from slip to stick due to the tangential contact stiffness. Because of the stochastic component of the friction coefficient the displacement for the transition from stick to slip is not constant. Figures 29(b) and 29(c) show higher periodic orbits.

The stochasticity of the measured signals is handled in the following way: The displacements in the transition regime $x_{A,\min} < x < x_{A,\max}$ are divided into K classes of the width $B = (x_{A,\max} - x_{A,\min})/K$. So, the probability p of a transition point from stick to slip in the Lth class results from the ratio of the number of transition points in the class L to the number of measured transition points (here ~ 300), see Figure 30. Due to the non-linearity the probability distribution in Figure 30(d) is not Gaussian.

Following this way of handling the measured data a bifurcation diagram has been measured, [Figure 31(a)]. In this diagram with the excitation frequency as bifurcation parameter the probability is visualized by means of the given colour code. Black marked regions correspond to transition domains with high probability, a transition point in the light grey marked regions occurs with low probability.

In Figure 31(a) there are three islands with a small transition domain. Two islands overlap for 7 [1/s] $< \Omega <$ 9 [1/s]. For $\Omega >$ 9 [1/s] the transition domain of the first island is left and the solution jumps completely to the domains in the second island. For $\Omega >$ 16 [1/s] the transition from stick to slip takes place in the interval between $x = 0{\cdot}1$ [mm] and $x = 0{\cdot}5$ [mm]. The results from the simulations [Figure 31(b)] also predict the three islands that are inclined, so the displacements decrease for increasing Ω. For $\Omega = 9{\cdot}75$ [1/s] there is a higher periodic solution with overlapping islands. In the range of $\Omega > 16{\cdot}5$ [1/s] the transition from stick to slip takes place in the interval between $x = 0{\cdot}1$ [mm] and $x = 0{\cdot}45$ [mm]. A more detailed insight into the different solutions and a discussion of the winding number can be found in reference [5].

So, by means of the proposed extensions of the mechanical model and the friction model it is possible to describe the bifurcational behaviour observed in the experiments.

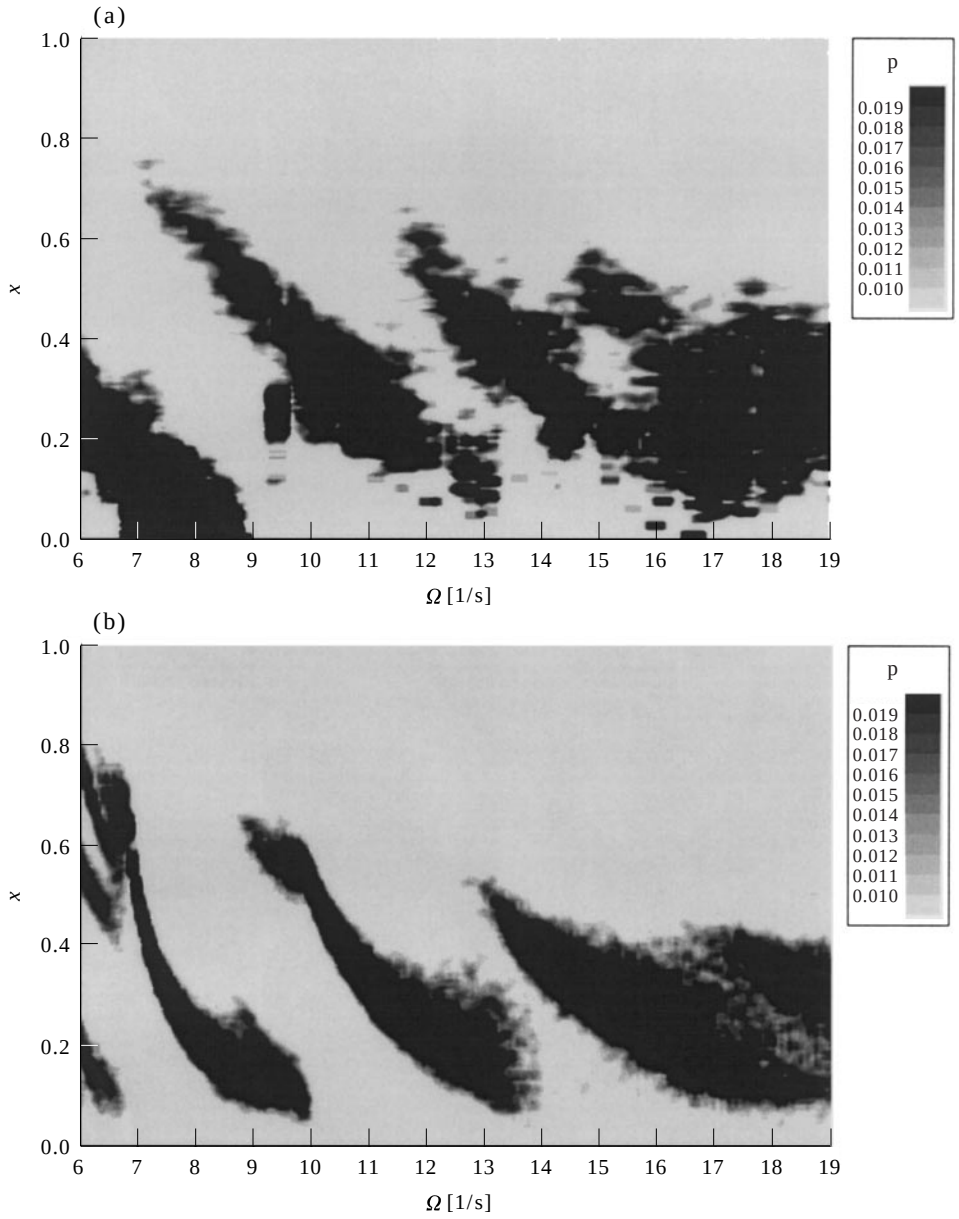

Figure 31. Bifurcation diagram of the friction oscillator with simultaneous self- and external excitation: (a) measurement, (b) simulation ($c_R = 4\,000\,000$ [N/m], $b_R = 400$ [Ns/m], $\mu_0 = 0{\cdot}8$, $\mu = 0{\cdot}55$, $F_N = 14$ [N], $u_0 = 0{\cdot}0005$ [m], $\sigma = 0{\cdot}015$).

9. CONCLUSIONS

Based on a linear model for the mechanical oscillator and a non-smooth friction model for the contact, the dynamics of the non-smooth system have been investigated numerically for pure self excitation, pure external excitation and simultaneous self- and external excitation. In the presence of the external excitation rich bifurcational behaviour can be observed, which shows a sensitive

dependence on the bifurcation parameters. The results for the three types of excitation have been verified experimentally, also bifurcation diagrams have been measured for the friction oscillator with external excitation and simultaneous self- and external excitation. For the prediction of the period and the amplitude of the solutions in the investigated parameter region the simple model of a friction oscillator is accurate enough and easy to implement to the numerics. However, a more detailed look shows that stochastic features of the signal and oscillations at the non-smooth transition points observed in the experiments cannot be predicted. More accurate are the simulation results on the basis of a bristle model proposed in reference [6] that models the elastic and plastic deformations of the contacting asperities. The solution procedure for the bristle model, however, demands large computation times. More efficient are two simplified models comprising the required stochastic features and the dynamics in the transition regimes. The first one, also investigated in reference [13], reduces the large number of bristles to one tangential contact spring and damper; the second simplification adds a stochastic component to the deterministic friction coefficient. The choice of the appropriate model has to obey the well-known rule that the model should be complex enough to cover the phenomena, but should be as simple as possible.

REFERENCES

1. K. Popp, N. Hinrichs and M. Oestreich 1995 *Sãdhanã* **20**, Part 2–4, 627–654. Dynamical behaviour of a friction oscillator with simultaneous self and external excitation.
2. P. Stelter 1990 *Nichtlineare Schwingungen reibungserregter Strukturen*, Fortschr.-Ber. VDI-Reihe 11, 137. Dûsseldorf: VDI-Verlag.
3. J. P. Den Hartog 1931 *Transactions ASME*, *APM*-53-9, 107–115. Forced vibrations with Coulomb and viscous friction.
4. S. W. Shaw 1986 *Journal of Sound and Vibration* **108**, 305–325. On the dynamic response of a system with dry friction.
5. M. Oestreich, N. Hinrichs and K. Popp 1996 *Archive of Applied Mechanics* **66**, 301–314. Bifurcation and stability analysis for a non-smooth friction oscillator.
6. N. Hinrichs, M. Oestreich and K. Popp 1997 *Chaos*, *Solitons & Fractals* **8**(3), (special issue: Guest editor T. Kapitaniak: Nonlinearities in applied engineering systems). Dynamics of oscillators with impact and friction.
7. N. Hinrichs 1997 *Ph.D. Thesis*, *University of Hannover*. Reibungsschwingungen mit Selbst- und Fremderregung: Experiment, Modellierung und Berechnung.
8. N. Hinrichs, M. Oestreich and K. Popp 1996 *Z. angew. Math. Mech.* **76**, 205–206. Coexisting periodic solutions of a non-smooth friction oscillator.
9. H. D. I. Abarbanel 1995 in *Smart Structures*, *Nonlinear Dynamics*, *and Control*, 1–86. New Jersey: Prentice Hall PTR. Tools for analysing observed chaotic data.
10. M. Oestreich, N. Hinrichs and K. Popp 1996 *Proc. of IMECE*: *Elasto-Impact and Friction in Dynamic Systems* **90**, 1–8. Signal and model based analysis of systems with friction and impacts.
11. N. Hinrichs, M. Oestreich and K. Popp 1996 *Proc. of IMECE*: *Elasto-Impact and Friction in Dynamic Systems* **90**, 57–62. Experimental and numerical investigation of a friction oscillator.
12. A. Soom and C.-H. Kim 1981 *ASME*: 81-*DET*-40. The measurement of dynamic normal and frictional contact forces during sliding.

13. B. F. Feeny 1996 *Proc. ASME: IMECE: Elasto-Impact and friction in dynamic systems* (DE-Vol. 90), 85–96. The effects of tangential contact stiffness on a harmonically forced friction oscillator.
14. B. N. J. Persson 1994 *Physics Review B*. **50**(7), 4771–4786. Theory of friction: The role of elasticity in boundary lubrication.
15. H. A. Sherif 1991 *Wear* **141**, 227–234. Effect of contact stiffness on the establishment of self-excited vibrations.
16. D. A. Haessig and B. Friedland 1991 *Transactions ASME: Journal Dynamic Systems, Measurement and Control* **113**, 354–362. On the modeling and simulation of friction.
17. P. Vielsack 1996 *Z. angew. Math. Mech.* **76**(8), 439–446. Regularisierung des Haftzustandes bei Coulombscher Reibung.